

Computation of Oxidation Potentials of Solvated Nucleobases by Static and Dynamic Multilayer Approaches

Jesús Lucia-Tamudo,[†] Gustavo Cárdenas,[†] Nuria Anguita-Ortiz,[†] Sergio Díaz-Tendero,^{*,†,‡,¶} and Juan J. Nogueira^{*,†,‡}

[†]*Department of Chemistry, Universidad Autónoma de Madrid, 28049, Madrid, Spain*

[‡]*Institute for Advanced Research in Chemistry (IAdChem), Universidad Autónoma de Madrid, 28049 Madrid, Spain*

[¶]*Condensed Matter Physics Center (IFIMAC), Universidad Autónoma de Madrid, 28049 Madrid, Spain*

E-mail: sergio.diaztendero@uam.es; juan.nogueira@uam.es

Abstract

The determination of the redox properties of nucleobases is of paramount importance to get insight into the charge-transfer processes in which they are involved, as those occurring in DNA-inspired biosensors. Although many theoretical and experimental studies have been conducted, the value of the one-electron oxidation potentials of nucleobases is not well defined. Moreover, the most appropriate theoretical protocol to model the redox properties has not been established yet. In this work, we have implemented and evaluated different static and dynamic approaches to compute the one-electron oxidation potentials of solvated nucleobases. In the static framework, two thermodynamic cycles have been tested to assess their accuracy against the direct

determination of oxidation potentials from the adiabatic ionization energies. Then, the introduction of vibrational sampling, the effect of implicit and explicit solvation models, and the application of the Marcus theory have been analyzed through dynamic methods. The results revealed that the static direct determination provides more accurate results than thermodynamic cycles. Moreover, the effect of sampling has not shown to be relevant, and the results are improved within the dynamic framework when the Marcus theory is applied, especially in explicit solvent, with respect to the direct approach. Finally, the presence of different tautomers in water does not affect significantly the one-electron oxidation potentials.

1 Introduction

The determination of the one-electron redox potentials of the nucleobases by experimental measurements is a very difficult task due to the irreversibility of the process and the low solubility of some nucleobases in water.¹⁻⁶ In the same way, the computation of the potentials is also challenging due to the several factors that can be considered in the theoretical model by means of different approaches, such as vibrational sampling, solvent effects and the level of theory at which the electronic structure of the nucleobases are described. However, an accurate characterization of the redox properties of nucleobases is crucial to understand the molecular mechanism of different charge-transfer processes in which the DNA constituents are involved, as those occurring in biosensor devices.^{7,8} DNA-based biosensors have been proved to be a convenient choice when trying to detect specific sequences of nucleic acids due to the DNA capability of hybridization.⁹⁻¹³ Recently, these devices have been also employed as nanowires or for the detection of organic analytes and heavy metals.^{9,14-16} In order to carry out the detection task, charge-transfer processes often play an important role and the nucleobase moiety has been shown to be the main constituent of the nucleotides that is involved in these phenomena.¹ Thus, the attainment of the redox properties of nucleobases is fundamental to get insight into the functioning mechanism of DNA-based biosensors.

This work is aimed to establish the most appropriate computational strategy to evaluate the one-electron oxidation potential of the five nucleobases present in DNA and RNA, by combining different theoretical models, and compare the results with the data available in the literature. We will use the term "one-electron oxidation potential" as the potential of the oxidation process but considered in the direction of a reduction reaction. Thus, the "one-electron oxidation potential" is a reduction potential as it is usually considered in the literature by convention. Many different experiments have been performed during the last decades, leading to a large variety of results. For example, Faraggi and co-workers employed cyclic voltammetry, differential pulse polarography and pulse radiolysis to determine the oxidation potentials at different pH values.³ Jovanovic and Simic employed pulse radiolysis to obtain the oxidation potentials at pH=13.0.⁴ Jovanovic also conducted further experiments with Steenken and determined the oxidation potential for guanine using kinetic rate measurements at physiological pH.^{17,18} Analogously, Steenken also obtained these values for the rest of nucleobases, which were supported by Burrows and co-workers.^{19,20} Seidel and co-workers performed fluorescence quenching experiments to determine the potentials in acetonitrile,⁵ and compared them with those reported in aqueous solution by Kittler and co-workers at pH=6.5.²¹ As can be seen in Table 1, all these experimental studies have provided a large range of one-electron oxidation potentials for the five nucleobases.

Table 1: Experimental^{3-5,17-23} and theoretical^{1,2,24-30} ranges provided by the literature for one-electron oxidation potentials of the nucleobases in aqueous solution.

Nucleobase	Experiment/V	Theory/V
Adenine	1.20–1.63	1.38–2.22
Cytosine	1.44–1.86	1.76–2.50
Guanine	0.80–1.53	1.10–1.88
Thymine	1.29–1.73	1.42–2.46
Uracil	1.34–1.75	1.62–2.57

From the computational perspective, many studies based on static and dynamic approaches have also been developed with the aim of computing the redox properties of nu-

cleobases. For example, within a static picture, Baik *et al.* determined the one-electron oxidation potentials for the nucleobases from the adiabatic ionization energies (AIE, see Figure 1a) computed by density functional theory (DFT) combined with a continuum-solvent approach.²⁵ Thapa and Schlegel²⁷ simulated the methyl-substituted nucleobases and some of their tautomers using also a DFT/continuum-solvent approach and taking into account the contribution of the formation of the solvated electron. Crespo-Hernández and co-workers³¹ evaluated if there was a correlation between the calculated vertical ionization energy (VIEs) or the vertical electron affinity (VEAs) using DFT/continuum models and the redox potentials of twenty organic molecules, for which their experimental redox potentials were well-known in acetonitrile. After obtaining a linear correlation, they used such a relation to obtain the redox properties of nucleobases in acetonitrile through the calculated VIEs and VEAs. On the other hand, Li *et al.* designed a protocol to investigate aromatic compounds, including the nucleobases,²⁴ which consists of a thermodynamic cycle and computations based on DFT and continuum solvent models. In such a protocol, solvation and structural relaxation effects were determined separately. Paukku and Hill²⁸ and Lewis *et al.*²⁹ determined the redox potentials of nucleobases based on the same thermodynamic cycle but using a different level of theory and continuum solvation models. They also compared the VIEs with the AIEs, and the VEAs with the adiabatic electron affinities (AEAs), properties intimately related with the oxidation and reduction potentials (see Figure 1a). Psciuk and co-workers² computed the redox potentials of the methyl-substituted nucleobases using the same strategy, but they took into account the different tautomers of the nucleobases that can be present in a protic solvent as water.

The one-electron oxidation potentials of nucleobases have also been computed based on dynamic approaches, specifically, using classical molecular dynamics (MD)^{32,33} or quantum mechanics/molecular mechanics MD³⁴ (QM/MM MD) simulations. In this context, Wang and co-workers³⁰ evolved classical MD trajectories for all the nucleobases in order to obtain an appropriate ensemble of conformational configurations of the molecules in aqueous phase

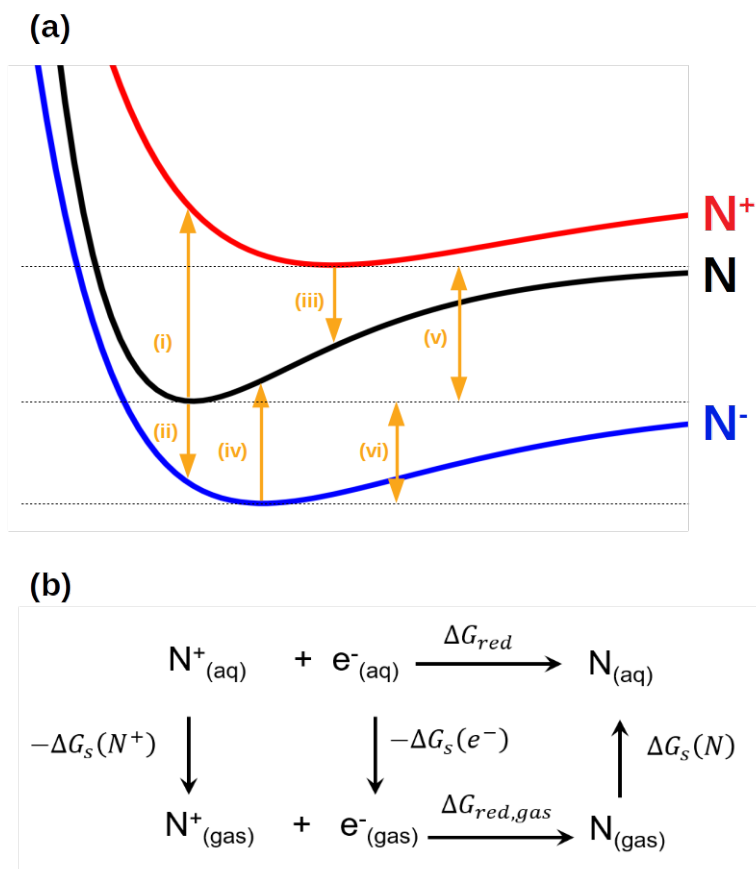


Figure 1: (a) Schematic representation of the different energetic related with reduction and oxidation processes: (i) Vertical ionization energy (VIE), (ii) vertical electron affinity (VEA), (iii) vertical attachment energy (VAE), (iv) vertical detachment energy (VDE), (v) adiabatic ionization energy (AIE), (vi) adiabatic electron affinity (AEA). (b) Thermodynamic cycle to compute reduction free energy in solvent ΔG_{red} from the solvation free energies of the oxidized species $\Delta G_s(\text{N}^+)$, reduced species $\Delta G_s(\text{N})$, and electron $\Delta G_s(\text{e}^-)$, and the reduction free energy in the gas phase $\Delta G_{\text{red,gas}}$.

using the TIP3P³⁵ force field for the description of water. Then, from different snapshots, QM/MM MD simulations were performed in order to relax the nucleobase geometries, and finally the VIEs, VEAs and vertical detachment energies (VDEs) were obtained by DFT/MM calculations, from which the redox potentials were determined. Zhang *et al.*²⁶ followed a similar methodology but they used QM/MM MD simulations to relax the neutral, cationic and anionic species starting from snapshots taken from a classical MD simulation of the neutral species. Then, VIEs, VEAs, AIEs, AEAs and VDEs were computed by means of a DFT/MM approach. All these energetic terms are schematically represented in Figure 1a. Recently, D’Annibale *et al.*¹ reported the redox properties of nucleobases and nucleosides by using an innovative methodology. In a first step, they conducted classical MD simulations to obtain a full ensemble of geometries of the neutral and cationic forms of the nucleobases in aqueous solvation. Then, in a second step, they performed DFT/MM calculations using the perturbed matrix method.^{36,37} Finally, they applied Marcus theory to estimate the one-electron oxidation potentials using the VIEs and the vertical attachment energies (VAEs). As in the case of the experimental measurements, the computed oxidation potentials listed in Table 1 lie in a large range of values. Moreover, they are considerably larger than the experimental potentials. Thus, a clear value for the one-electron oxidation potentials of the nucleobases can not be extracted from the literature.

In spite of all the previously mentioned efforts, it is still not clear which methodology is more appropriate to compute the redox potentials for the nucleobases and, in general, for organic molecules. In fact, the use of thermodynamic cycles has been recently compared with the direct determination of the reduction potentials from the AIEs for different molecules, and a general conclusion could not be drawn.³⁸ In addition, the calculation of redox properties in solvent or in biological media also requires an accurate description of the environment in terms of both interactions and sampling. In this work, we have computed the one-electron oxidation potentials of the five nucleobases in water using different protocols and theoretical models within static and dynamic frameworks aimed to different goals: (i) to compare

the use of two different thermodynamic cycles with the direct determination of the oxidation potentials from the AIEs within a static framework; (ii) to evaluate the introduction of sampling effects and compare two different dynamic protocols where the potentials are computed from the AIEs and by the Marcus theory; (iii) to investigate the effect of solvent models using implicit (COSMO) and explicit (TIP3P) solvation; (iv) to assess the accuracy of different DFT functionals for each of the static and dynamic protocols; and (v) to evaluate the importance of considering different tautomeric species.

2 Methods

2.1 Static Approaches

The reduction free energy of the process shown in Figure 1b can be written as the free energy difference between the solvated reduced and oxidized species as:

$$\Delta G_{red} = G(N_{(aq)}) - G(N_{(aq)}^+) - \Delta G_s(e^-) \quad (1)$$

where the free energy of each individual species can be written as the summation of the electronic energy E_e and the thermal correction to the Gibbs free energy G_T , which includes electronic, translational, rotational, and vibrational contributions. Both energy terms are usually computed by using a continuum solvent approach, such as the polarizable continuum model (PCM)³⁹⁻⁴⁴ or the Conductor-like Screening model (COSMO).^{45,46} Thus, Eq. 1 can be written as:

$$\Delta G_{red} = E_e(N_{(aq)}) + G_T(N_{(aq)}) - E_e(N_{(aq)}^+) - G_T(N_{(aq)}^+) - \Delta G_s(e^-) \quad (2)$$

where the solvation free energy of the electron is $\Delta G_s(e^-) = -0.867$ kcal/mol^{47,48} and must be taken into account since the reduction potential values of the reference electrodes also

account for it. The reduction potential E_{red} is related to the free energy as follows:

$$\Delta G_{red} = -nFE_{red} \tag{3}$$

where F is the Faraday constant and n is the number of exchanged electrons. Typically, redox potentials are given with respect to a reference potential. A common choice as reference is the standard hydrogen electrode (SHE), whose reduction potential is $E_{red,SHE}^0 = 4.281 \text{ V}$.⁴⁹⁻⁵² Thus, the reduction potential relative to the SHE value reads as:

$$\Delta E_{red}^0 = \frac{\Delta G_{red}}{nF} - E_{red,SHE}^0 \tag{4}$$

The use of Eqs. 1-4 to obtain the reduction potentials is termed here as static direct calculation. In this methodology, the terms E_e and G_T for the reduced and oxidized species in Eq. 2 are computed at their corresponding optimized geometries in a continuum solvent model. In other words, the free energy of the reduction process is obtained from the AIE (see Figure 1a).

It has been recently stated that the use of the static direct recipe can lead to errors in the determination of the free energy.³⁸ Specifically, the calculation of the thermal correction G_T in a continuum solvent is not completely correct. First, continuum models have been parameterized so that the electronic energy E_e of the solute including the interaction with the solvent reproduces the experimental solvation energy. Therefore, thermal effects are already included implicitly in E_e and the computation of G_T in the continuum solvent model double counts these effects. Second, the ideal-gas partition functions employed when computing the thermal corrections for the solvated species are not correct in solvent. Consequently, it has been suggested that the use a thermodynamic cycle, where the thermal corrections are computed in the gas phase, is more accurate.

The free energy of the reduction reaction can also be expressed by using the thermody-

namic cycle shown in Figure 1b as:

$$\Delta G_{red} = \Delta G_{red,gas} - \Delta G_s(N^+) - \Delta G_s(e^-) + \Delta G_s(N) \quad (5)$$

where $\Delta G_s(I)$ is the solvation free energy of the species I and $\Delta G_{red,gas}$ is the free energy of the reduction process in the gas phase. The last one can be written as the summation of electronic E_e and thermal correction G_T contributions:

$$\Delta G_{red,gas} = E_e(N_{(gas)}) + G_T(N_{(gas)}) - E_e(N_{(gas)}^+) - G_T(N_{(gas)}^+) \quad (6)$$

In addition, the solvation free energy $\Delta G_s(I)$ is calculated as the difference between the electronic energy of the solute in solvent and in the gas phase:

$$\Delta G_s(N^+) = E_e(N_{(aq)}^+) - E_e(N_{(gas)}^+) \quad (7)$$

$$\Delta G_s(N) = E_e(N_{(aq)}) - E_e(N_{(gas)}) \quad (8)$$

By using the above described thermodynamic cycle, the thermal corrections are computed in the gas phase though the terms $G_T(N_{(gas)})$ and $G_T(N_{(gas)}^+)$ in Eq. 6, where the ideal-gas partition functions are correct, and corrections to the thermal energy due to the discrepancies between the solvent phase and the gas phase are considered in the computation of the electronic energies through Eqs. 7 and 8.

In this work, two different versions of the thermodynamic cycle have been tested. In the first one (static cycle 1), the solvation free energies $\Delta G_s(N)$ and $\Delta G_s(N^+)$ are evaluated with the geometries of the reduced and oxidized species optimized in solvent and in the gas phase, i.e., the geometry relaxation of the solute upon solvation is considered. In the second version (static cycle 2) the solvation free energies of Eqs. 7 and 8 are computed by employing the relaxed geometry in the gas phase. This second approximation does not take into account the relaxation of the solute in solvent, but it is still often found in the

literature because it avoids the geometry optimization in continuum solvation models, where convergence is sometimes difficult to achieve.^{29,31}

2.2 Dynamic Approaches

The reduction potentials can also be determined by using dynamic methodologies where conformational motion (sampling) is introduced in the theoretical model. Warshel proposed a methodology that allows the computation of free energies using trajectories for donor-acceptor couples,^{53,54} and Blumberger *et al.* applied this approach to redox half reactions.⁵⁵ The free energy of a reaction, for example, a reduction process, is related to the Helmholtz energy ΔA_{red} by:

$$\Delta G_{red} = \Delta A_{red} + p\Delta V_{red} \quad (9)$$

where p is the pressure and ΔV_{red} is the change of volume during the reaction. For reactions in which the volume modification is negligible $\Delta G_{red} = \Delta A_{red}$. It can also be proved that the Helmholtz energy of the species I can be computed from the ensemble average of its potential energy as:⁵⁶

$$A_I = -k_B T \ln \left\langle e^{\frac{-E_I\{\mathbf{r}\}}{k_B T}} \right\rangle_I \quad (10)$$

being k_B and T the Boltzmann constant and temperature, respectively, and \mathbf{r} represents the coordinates of the system. Assuming that $\Delta V_{red} = 0$ and introducing Eq. 10 into Eq. 1, the reduction free energy can be expressed in terms of ensemble averages:

$$\Delta G_{red} = -k_B T \ln \left\langle e^{\frac{-E_N\{\mathbf{r}\}}{k_B T}} \right\rangle_N + k_B T \ln \left\langle e^{\frac{-E_{N^+}\{\mathbf{r}\}}{k_B T}} \right\rangle_{N^+} - \Delta G_s(e^-) \quad (11)$$

where the subscripts of the brackets indicate the phase space where the potential energy average is computed. Thus, the ensemble average of the potential energy of the reduced species N in the first term of Eq. 11 is computed in the phase space of N , while the ensemble average of the potential energy of the oxidized species N^+ in the second term

of Eq. 11 is computed in the phase space of N^+ . The ensemble averages for each of the species can be easily determined by running classical MD simulations for each phase space, selecting several snapshots and computing the potential energy for the selected snapshots by QM/MM or QM/continuum approaches, where the solute is included in the QM region and the solvent is described by a MM force field or by a continuum model. Finally, the average of the potential energies for each ensemble is introduced in Eq. 11 and the free energy is obtained. We will refer to this methodology as dynamic direct explicit or dynamic direct implicit approach, depending on the solvent model employed in the potential-energy calculations.

Reduction potentials can also be computed by using the Marcus theory, where sampling and environmental effects are included. Eq. 11 can be rewritten in the following way:

$$\begin{aligned}\Delta G_{red} &= -k_B T \ln \left\langle e^{\frac{\Delta E_{N \rightarrow N^+}(\mathbf{r})}{k_B T}} \right\rangle_N - \Delta G_s(e^-) = \\ &= -k_B T \ln \left\langle e^{\frac{-\Delta E_{N^+ \rightarrow N}(\mathbf{r})}{k_B T}} \right\rangle_{N^+} - \Delta G_s(e^-)\end{aligned}\tag{12}$$

where $\Delta E_{N \rightarrow N^+}(\mathbf{r})$ and $\Delta E_{N^+ \rightarrow N}(\mathbf{r})$ are the VIE and the VAE, respectively, computed on the appropriate ensemble of N or N^+ . Assuming that the solvent response is linear with respect to a change in the solute, Marcus theory can be applied.⁵⁷⁻⁶¹ Hence, both the distributions of VIEs and VAEs will be Gaussian functions and their standard deviations will be the same. Under these circumstances Eq. 12 can be simplified to:

$$\begin{aligned}\Delta G_{red} &= \frac{1}{2} \left(\langle \Delta E_{N \rightarrow N^+}(\mathbf{r}) \rangle_N - \langle \Delta E_{N^+ \rightarrow N}(\mathbf{r}) \rangle_{N^+} \right) - \Delta G_s(e^-) = \\ &= \frac{1}{2} \left(\langle VIE \rangle_N - \langle VAE \rangle_{N^+} \right) - \Delta G_s(e^-)\end{aligned}\tag{13}$$

In order to compute $\langle VIE \rangle_N$ ($\langle VAE \rangle_{N^+}$), classical MD simulations are run for the reduced species N (oxidized species N^+) in its own phase space. Then, several snapshots are chosen along the dynamics and for those selected snapshots the VIEs (VAEs) are calculated by QM/MM or QM/continuum approaches, where only the solute is included in the QM region

(see Figure 2). Finally, the VIEs (VAEs) values are averaged. Depending on the solvent model employed in the VIE (VAE) computations this methodology will be named dynamic Marcus explicit or dynamic Marcus implicit approach.

3 Computational Details

3.1 Static Calculations

All the QM, QM/continuum and QM/MM calculations were performed using the NWChem package.⁶² Three different functionals were tested within the static and dynamic methodologies: PBEOP,^{63–65} which provided previously accurate results for nucleobases,⁶⁶ and the B3LYP^{67–70} and M06-2X⁷¹ functionals, widely employed in the computation of ground-state properties. The selected basis set was 6-311G(d).^{72,73}

All the nucleobases were optimized in their neutral and cationic forms in both gas phase and aqueous phase using the three functionals and the basis set mentioned above. The optimization of the cationic form of cytosine did not converge for B3LYP and M06-2X. In these cases, the optimized geometries of the neutral and cationic cytosine using PBEOP were used in order to compute the energy of the system with B3LYP and M06-2X. The aqueous solvent in the QM/continuum calculations was described by COSMO.^{45,46} A frequency calculation was performed for each geometry to ensure that an energy minimum was reached and to compute the zero-point energy, which is part of the thermal correction. By calculating the energy of the cationic and neutral species in both the gas phase and in solvent, the oxidation potentials for the three different models described above are obtained: static direct, static cycle 1 and static cycle 2 approaches.

3.2 Dynamic Calculations

Classical MD simulations were run with the AMBER20 package⁷⁴ and the systems were built up with AmberTools 20⁷⁴ and different homemade scripts. For both the cation and the

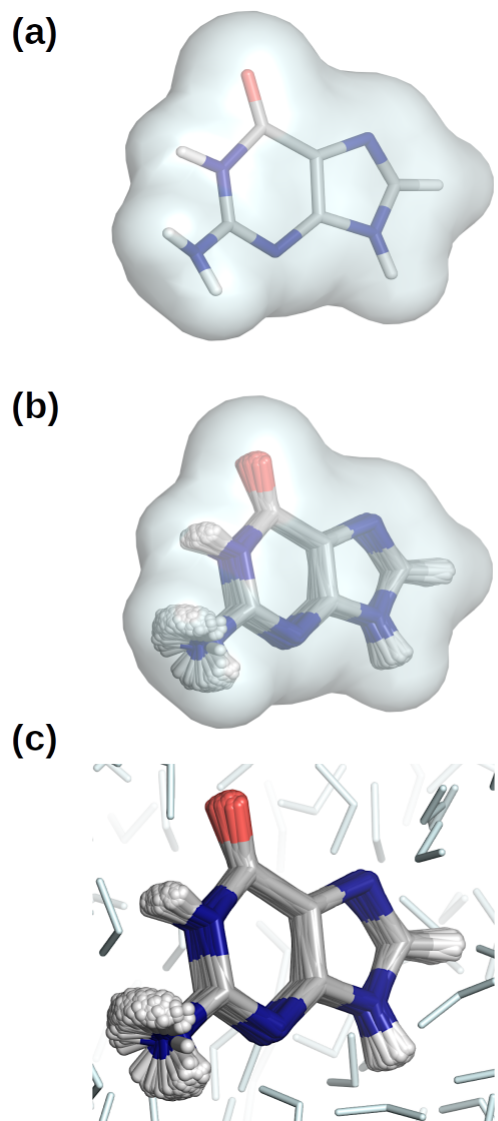


Figure 2: Representation of the different types of calculations performed. (a) Static calculations in which the solvent is described by the continuum COSMO solvation model. (b) Dynamic calculations in which the sampling of the solute is taking into account and the solvent is described by COSMO as in (a). (c) Dynamic calculations in which the sampling of the solute and solvent is taking into account since the solvent is described explicitly with TIP3P. Several frames have been aligned to represent the vibrational motion of the solute in (b) and (c). Color code: N in blue, C in grey, O in red, H in white and solvent (water) in light blue.

neutral forms of each nucleobase, three different sets of force field parameters were developed, based on quantum mechanic calculations performed with the PBEOP, B3LYP M06-2X functionals, by the following procedure. First of all, the Hessian matrix for the optimized geometries obtained in the static calculations in aqueous phase was computed. Bond and bond angle parameters for the nucleobases were obtained from the Hessian matrix by the Seminario method using each of the considered functionals.⁷⁵ Parameters for dihedral angles, improper torsions and Lennard–Jones non-bonded terms were taken from the generalized Amber force field (GAFF).⁷⁶ Electrostatic potential (ESP) charges were obtained from a DFT calculation in aqueous phase. Each nucleobase was solvated in a tetragonal simulation box of around (60 x 57 x 61) Å³ with approximately 17000 water molecules, which were described with the TIP3P solvation model.³⁵ For the cationic form, a chloride anion was also added to neutralize the system, described by the Joung and Cheatham parameters.⁷⁷

After the setup of the different systems, the same dynamic protocol was followed for all of them. First, the system was minimized for 10000 steps in which the steepest descent algorithm⁷⁸ was used for the 5000 first steps and the Newton-Raphson algorithm⁷⁹ for the last 5000 steps. After that, a constant volume (NVT) progressive heating to 300 K was performed for 500 ps. The Langevin thermostat was applied to control the temperature with a collision frequency of 2 ps⁻¹. Then, an additional 500 ps simulation was run at 300 K in the NVT ensemble. Afterwards, a 1 ns simulation was run in the NPT ensemble to equilibrate the volume of the system and reach the correct density. Finally, a 500 ns production simulation was run in the NPT ensemble. The Berendsen barostat with isotropic position scaling and a pressure relaxation time of 2 ps was employed to maintain the pressure constant at 1 bar. During the full protocol the particle-mesh Ewald method⁸⁰ with a grid spacing of 1.0 Å was used to compute the electrostatic interactions and a 10 Å cutoff for the nonbonded interactions was chosen. The SHAKE algorithm^{81–83} restrained the bonds involving hydrogen atoms and a time step of 2 fs was used during the heating, equilibration and production stages.

For each cationic and neutral trajectory of the five nucleobases, 200 snapshots were fetched randomly from the last 450 ns of the production trajectories. In the case of the snapshots of the neutral species the VIEs were computed by running QM/TIP3P and QM/-COSMO calculations. For the QM/COSMO calculations the explicit solvent molecules were removed from the different snapshots and replaced by COSMO. Regarding the cationic trajectories the VAEs were computed also by QM/MM and QM/COSMO calculations in the same way. These calculations were run for the three functionals and basis set described above for the static approaches. Since the optimization of the cationic cytosine molecule did not converge for B3LYP and M06-2X and, therefore, the Hessian matrix could not be obtained, the MD simulations of neutral and cationic cytosine with the force field parameters obtained from PBEOP were used in order to compute the energy of the system with B3LYP and M06-2X. All these calculations were combined as explained in the previous section to obtain the one-electron oxidation potentials for the dynamic direct implicit, dynamic direct explicit, dynamic Marcus implicit and dynamic Marcus explicit approaches.

4 Results

4.1 Static Protocols

We start the discussion by comparing the results from the three different stationary approaches described above: static direct, static cycle 1 and static cycle 2. The error of these three protocols for each of the five nucleobases employing the PBEOP, M06-2X and B3LYP functionals with respect to experimental measurements is shown in Figure 3. Specifically, due to the broad range of experimental values found in the literature, the unsigned error for each nucleobase is estimated as the absolute value of the difference between the computed oxidation potential and the average value of the experimental range listed in the second column of Table 1. In general, when comparing the results given by the different DFT functionals for all the nucleobases, PBEOP provides the most consistent potentials with respect

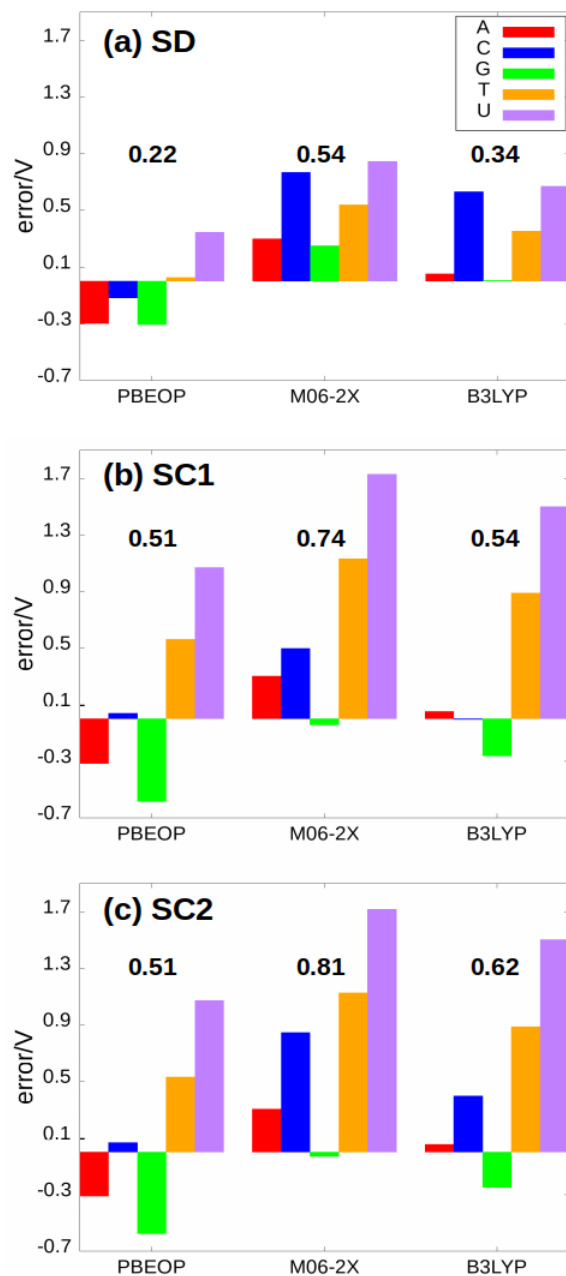


Figure 3: Errors of the calculated one-electron oxidation potentials for the five nucleobases obtained with the PBEOP, M06-2X and B3LYP functionals with respect to the reference experimental oxidation potentials using the three static protocols described in the text: (a) Static direct (SD), (b) static cycle 1 (SC1), (c) static cycle 2 (SC2). The values next to the bars are the MUEs for each functional. Color code: adenine (A) in red, cytosine (C) in blue, guanine (G) in green, thymine (T) in orange and uracil (U) in purple.

to the literature with mean unsigned errors (MUEs) of 0.22, 0.51 and 0.51 V for the static direct, static cycle 1 and static cycle 2 approaches, respectively. Moreover, the B3LYP and M06-2X functionals overestimate the potentials for all nucleobases but guanine, with MUEs lying within 0.34–0.62 V and 0.54–0.81 V for B3LYP and M06-2X, respectively. If Figure 3 is examined in more detail, one finds that the accuracy of the functionals is system dependent: the potential for adenine computed with B3LYP presents the lowest error for the three static protocols, the potential for guanine is more accurate when calculated with M06-2X, and for the pyrimidine nucleobases – cytosine, thymine and uracil – PBEOP is the most appropriate functional.

When comparing the three protocols, the static direct scheme is the one that provides the closest values with respect to the experiments for the three functionals (see Figure 3). This means that either the inaccuracies introduced in the thermal correction to the free energy when a continuum solvation model is used in the static direct protocol, as previously discussed,³⁸ are not important for the nucleobases or there exists error cancellation with other approximations inherent to the theoretical model employed. A more careful inspection of Figure 3 reveals that the determination of the one-electron oxidation potential for adenine seems to be invariant with respect to the theoretical protocol. In the case of cytosine, the static cycle 1 performs the best, although the static direct calculation with PBEOP provides a reasonable result with an error of ~ 0.3 V. The thermodynamic cycles completely fail when describing the oxidation potentials of thymine and uracil, presenting errors of ~ 0.9 V for thymine and ~ 1.3 V for uracil. The static cycle 2 scheme provides slightly higher MUE values than the static cycle 1, especially for cytosine. This shows that geometry relaxation when going from vacuum to solvent is relevant for cytosine, while the use of the vacuum geometries in COSMO calculations does not introduce significant errors for the other nucleobases. Overall, the best static strategy to compute the one-electron oxidation potential for the nucleobases has been proved to be the static direct method with the PBEOP functional.

4.2 Dynamic Protocols

The one-electron oxidation potentials have also been computed within a dynamic approach, where an ensemble of 200 geometries for each nucleobase, selected from classical MD simulations, were considered. Different factors that may influence the accuracy of the computations within this dynamic framework will be discussed in the following sections. First, it is important to achieve convergence with respect to the number of selected snapshots. Second, although the classical trajectories for sampling have been evolved in explicit solvation, the calculation of the oxidation potentials has been carried out in explicit and implicit models by using electrostatic embedding QM/MM and polarizable embedding QM/continuum schemes, providing potentials with different accuracy and convergence behaviour. Third, the free energy of the oxidation process for the different nucleobases has been obtained by applying the direct approximation, as in the static scenario, and the more sophisticated Marcus theory. Finally, the role of tautomers, which can be relevant in protic solvents such as water, have also been analysed.

4.2.1 Convergence of the Calculations

Figure 4 shows the evolution of the one-electron oxidation potentials with the number of snapshots considered for the five nucleobases computed by applying the direct and Marcus protocols with implicit COSMO and explicit TIP3P solvents. As can be seen, convergence is successfully reached for all the dynamic approaches when using 200 snapshots randomly fetched from the classical MD trajectories. However, the calculations performed with COSMO converge faster than those performed with TIP3P. Specifically, convergence is achieved for the continuum solvent after considering 40-60 snapshots, while it is necessary to average over around 100 snapshots to converge the oxidation potentials for explicit solvation. In addition, the oscillations of the average potentials are smaller for COSMO than for TIP3P. This is consistent with the fact that in the implicit solvation model the different configurations of the solvent are averaged in every calculation, while the solvent configura-

tion around the solute is different in each calculation with explicit solvent. Therefore, the variation of the oxidation potential along the different snapshots is larger in TIP3P because both the solute and solvent undergo important changes within the ensemble. Contrary, in the implicit calculations, only the solute geometry suffers important modifications and the cavity that represents the solvent adapts to these modifications with small deformations of its shape and tesserae charges.

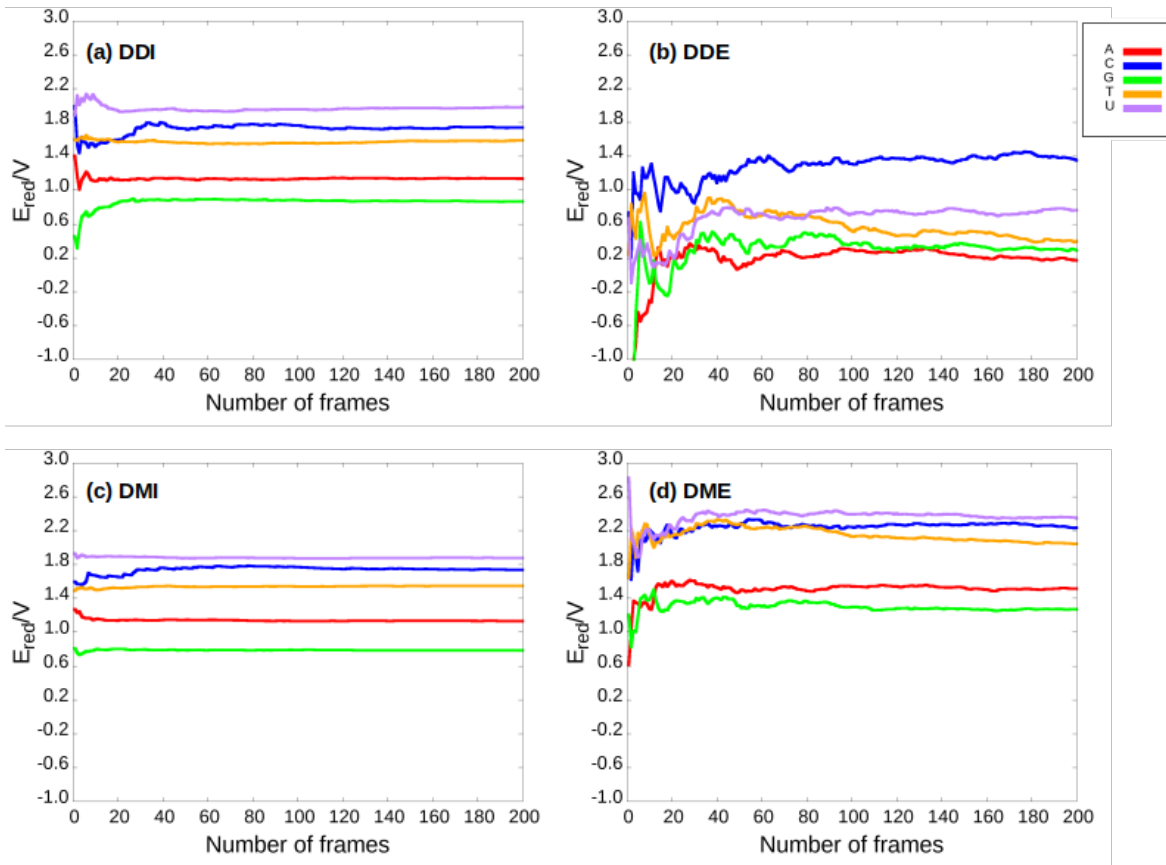


Figure 4: Evolution of the average one-electron oxidation potentials computed with PBEOP with respect to the number of frames for the five nucleobases using different dynamic protocols: (a) dynamic direct implicit (DDI), (b) dynamic direct explicit (DDE), (c) dynamic Marcus implicit (DMI), (d) dynamic Marcus explicit (DME). Color code: adenine (A) in red, cytosine (C) in blue, guanine (G) in green, thymine (T) in orange and uracil (U) in purple.

When comparing the dynamic direct with the dynamic Marcus approaches some differences can be observed (see Figure 4). First, convergence is reached with a smaller number of

snapshots when applying Marcus theory, especially when using the explicit TIP3P model as solvent. In addition, the oscillations observed for the Marcus theory are smaller than for the direct approach. This can be understood by realizing that the free energy of the oxidation process is computed as the average value of the VIE and VEA in the Marcus theory (see Eq. 13) and, thus, the number of single-point calculations employed in the dynamic Marcus protocols is double than that in the dynamic direct approaches (800 vs 400 single-point calculations for each nucleobase). The difference in the convergence behaviour between both dynamic protocols is almost negligible when using COSMO due to the averaging nature of the implicit model, as was explained above. In summary, the one-electron oxidation potential values converge for all the dynamic protocols when ~ 100 snapshots are used. However, convergence is achieved faster by applying Marcus theory and using the continuum solvent.

4.2.2 Effect of Sampling

The introduction of conformational sampling in the theoretical model may modify the properties of a system when compared with the static scenario.⁸⁴⁻⁸⁷ This arises from the fact that large sized systems do not present a single clear global minimum in their potential-energy surface but many local minima which are thermally accessible. As a result, static calculations only describe the properties of the system associated to one of these minima, whose selection is arbitrary. In these situations, there is a need to explore different conformations along the relevant regions of the potential-energy surface. This is achieved in the present work by running classical MD simulations.

In order to discuss the effect of sampling the errors in the one-electron oxidation potentials obtained by the static direct protocol with COSMO, displayed in Figure 3a, will be compared with those obtained by the dynamic direct implicit approach, shown in Figure 5a. The MUEs for the static direct approach are 0.22 V, 0.54 V and 0.34 V for PBEOP, M06-2X and B3LYP, respectively, while they are 0.24 V, 0.51 V and 0.32 V for the dynamic direct implicit approach. Therefore, static and dynamic oxidation potentials are very similar and,

thus, sampling effects are not relevant in this situation. The nucleobase that presents the most important variation in its potential when going from the static to the dynamic approach is cytosine, whose oxidation potential difference between both approaches is ~ 0.2 V. If the nucleobases are analysed individually, the introduction of sampling decreases (increases) the error of pyrimidines (purines), although these variations, as already said, are not important.

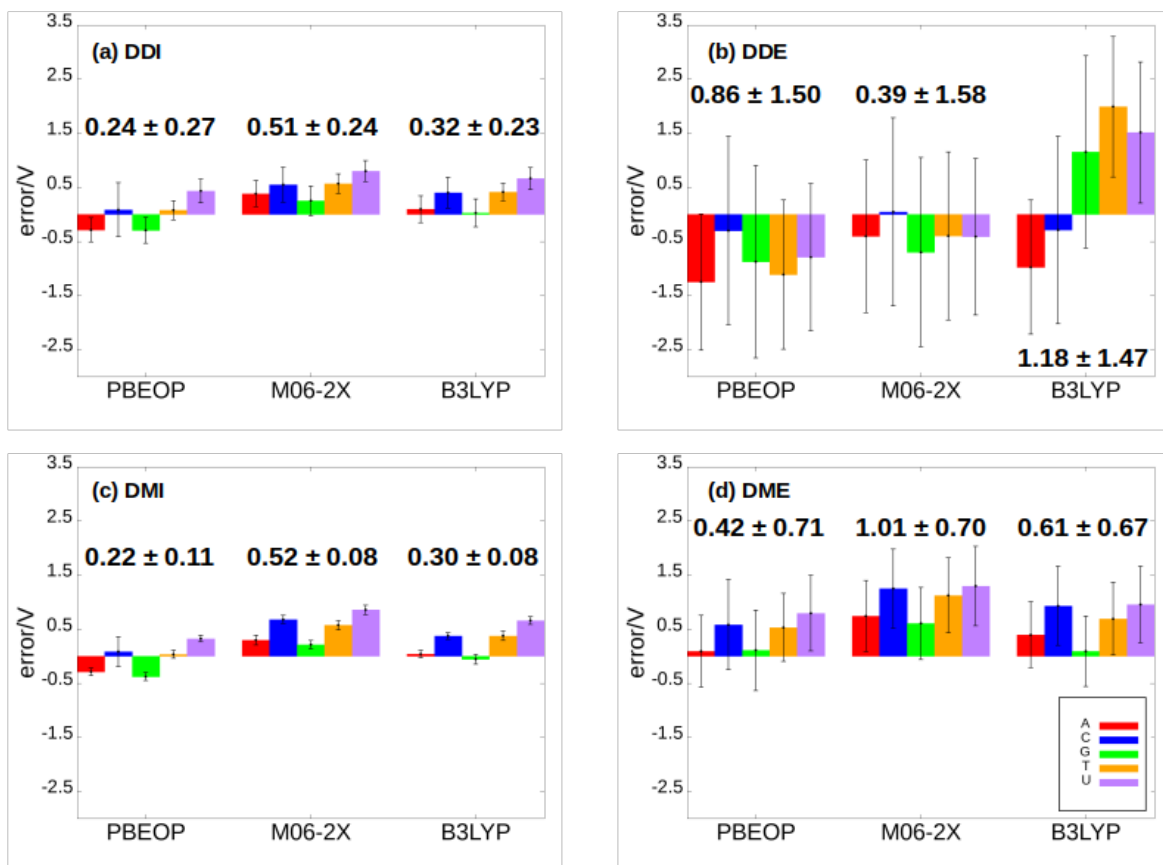


Figure 5: Errors of the calculated one-electron oxidation potentials for the five nucleobases obtained with the PBEOP, M06-2X and B3LYP functionals with respect to the reference experimental oxidation potentials using the four dynamic protocols described in the text: (a) Dynamic direct implicit (DDI), (b) dynamic direct explicit (DDE), (c) dynamic Marcus implicit (DMI), (d) dynamic Marcus explicit (DME). Error bars represent the standard deviation of the calculated potentials and the values next to the bars are the MAEs with their standard deviation for each functional. Color code: adenine (A) in red, cytosine (C) in blue, guanine (G) in green, thymine (T) in orange and uracil (U) in purple.

4.2.3 Effect of the Solvation Model

The presence of an environment, e.g., solvent, can also induce modifications in the molecular properties.^{85,88,89} Moreover, the magnitude of these modifications may be different depending on the solvent model employed. In the present work, two different solvent models have been investigated (see Figure 2), namely, the implicit COSMO and explicit TIP3P models. The effect of the solvent description on the oxidation potentials can be seen by doing the following comparisons: dynamic direct implicit (Figure 5a) vs dynamic direct explicit (Figure 5b) protocols and dynamic Marcus implicit (Figure 5c) vs dynamic Marcus explicit (Figure 5d) protocols. For both comparisons, it can be seen that the MUEs of the calculations performed with the explicit solvent are clearly larger than those of the calculations performed with COSMO. The only exception is found for the dynamic direct protocols employing the M06-2X functional, for which the MUE is 0.51 V for COSMO and 0.39 V for TIP3P. Therefore, in general, the one-electron oxidation potentials obtained with the implicit solvent model are more accurate than those obtained with the explicit one. At first glance, this could seem surprising since it is usually stated that explicit models are more accurate than implicit ones because specific interactions, such as hydrogen bonding, are taken into account. However, the effect of explicit solvent molecules is often introduced by an electrostatic-embedding QM/MM scheme, as was performed here, where the solvent molecules (MM region) polarize the solute (QM region) but the solvent is not polarized by the solute. In the case of implicit models, solvent effects are introduced by polarizable-embedding QM/continuum schemes, where there exists a mutual polarization between solute and solvent which, in principle, is more accurate than an electrostatic embedding. The fact that the COSMO calculations present a smaller error than the TIP3P ones indicates that, in the particular case of computing oxidation potentials for the nucleobases, polarization effects are more relevant than specific interactions, e.g., hydrogen bonding. Therefore, the use of the COSMO model to represent the water molecules is more appropriate than the use of TIP3P regarding the computation of oxidation potentials of nucleobases.

Another important difference found between the two solvent models is the variation of the oxidation potential along the snapshots of the ensemble. This is reflected in the standard deviations, which are represented in Figure 5 by the error bars. The standard deviations found in the explicit solvent calculations (0.42–1.58 V) are significantly larger than those for the implicit solvent calculations (0.08–0.27 V). As discussed above, this is explained by the nature of the implicit model, whose cavity represents an average situation of all possible solvent configurations. It is important to mention that, in principle, the larger standard deviation does not make TIP3P a worse model than COSMO. However, the large MUE values obtained with TIP3P demonstrate the worse performance of the explicit model.

4.2.4 Direct vs Marcus Theory Protocols

The application of the Marcus theory to compute the one-electron oxidation potentials could be thought to provide more accurate results than the direct protocol due to the greater complexity of the Marcus formulation. However, this is the case only when using explicit solvation but not implicit one. As can be seen in Figure 5a,c, the MUEs of the dynamic direct implicit approach are 0.24, 0.51 and 0.32 V for PBEOP, M06-2X and B3LYP, respectively, while similar MUE values are obtained for the dynamic Marcus implicit protocol (0.22, 0.52 and 0.30 V). Therefore, the accuracy of both dynamic procedures is very similar when using COSMO to reproduce solvent effects. In addition, these MUEs are also similar to the ones displayed in Figure 5a for the static direct (implicit) approach (0.22, 0.54 and 0.34 V). As was discussed in a previous section, sampling effects are not relevant in this particular situation. These three protocols (static direct implicit, dynamic direct implicit and dynamic Marcus implicit) present the best agreement with the experimental measurements, especially, when the PBEOP functional is used to describe the electronic structure of the nucleobases.

The situation is different for the explicit solvation calculations. The dynamic Marcus approach (Figure 5b) agrees better with the experiment than the dynamic direct approach (Figure 5d) for the PBEOP and B3LYP functionals, and the opposite is true for the M06-2X

functional. It is interesting to mention that the M06-2X functional also presents a smaller MUE in TIP3P (Figure 5b) than in COSMO (Figure 5a) for the dynamic direct protocol. Therefore, it seems that the results computed by M06-2X profit from error cancellation when this functional is combined with TIP3P in the dynamic direct approach. Nevertheless, despite the improvement of the results when applying Marcus theory with respect to the dynamic direct protocol in TIP3P for PBEOP and B3LYP, the most accurate results are still obtained for implicit solvation.

It is worthy to discuss some differences between the implicit and explicit solvent calculations within the dynamic framework. Figure 6 shows the different calculations which are involved in the dynamic direct and Marcus protocols. In these calculations, first, two different classical MD simulations are run for the neutral and the cationic nucleobases (represented by the black labels G and G⁺). In the case of the direct approach, the free energy of the oxidation process is obtained directly from the energy difference between the cationic and neutral trajectories. When the Marcus theory is instead applied, the VIE is computed from the neutral trajectory by removing an electron without relaxing the geometry, and the VAE is computed from the cationic trajectory by adding an electron without relaxing the geometry. These unrelaxed situations are represented in Figure 6 by the red labels G and G⁺. Finally, the oxidation free energy is computed as the average of the VIE and VAE. In the case of the explicit solvent calculations the same water molecules present in the dynamics are employed in the QM/MM energy calculations, while in the case of the implicit solvent calculations the explicit solvent molecules from the dynamics are replaced by the COSMO model in the QM/continuum energy calculations.

As can be seen in Figure 6, the unrelaxed geometries are higher in energy than the relaxed ones, as expected. As a consequence, the VIE is always higher than the VAE (5.30 vs 4.90 eV in COSMO and 8.09 vs 4.08 eV in TIP3P). However, the energy difference between the VIE and VAE is significantly larger in TIP3P than in COSMO because the energy difference between the relaxed and unrelaxed trajectories is also larger in the explicit solvent. This

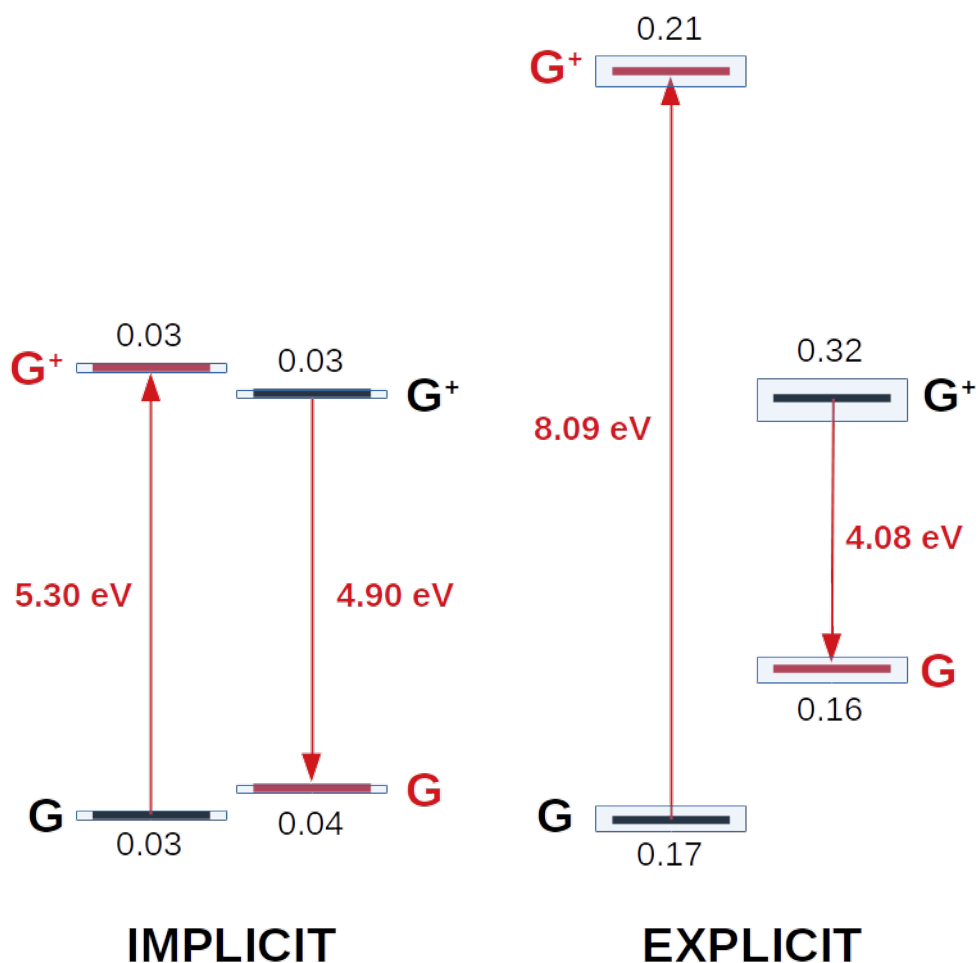


Figure 6: Schematic representation of the energy gaps employed in the dynamic direct and Marcus approaches using implicit and explicit solvation. The results shown were obtained for guanine with the PBEOP functional. Black labels (G and G⁺) represent geometrically relaxed species while red labels (G and G⁺) accounts for species whose energy was computed without geometry relaxation. Arrows pointing up and down represent the VIE and VAE, respectively. Blue boxes and black numbers account for the standard deviation of the energy of the correspondent state. All values are in eV.

can be rationalized as follows. When the VIE is computed by removing an electron from the snapshots of the neutral trajectory, in the COSMO solvent model the tesserae charges of the cavity change to adapt to the positive charge of the solute because of the existing mutual polarization between solute and solvent. Therefore, the reorganization of the solvent charges is stabilizing the unrelaxed geometry of the cationic nucleobase. As a result, the energy difference between the unrelaxed and the relaxed cationic solute is not too large. However, in the electrostatic-embedding QM/MM calculations with TIP3P, the charges of the solvent do not relax upon ionization of the neutral trajectory because TIP3P is a fixed-charge force field. Therefore, the energy of the unrelaxed cationic trajectory is much higher than the energy of the relaxed cationic trajectory. The same explanation holds for the VAE computation. When the cationic trajectory is neutralized, the unrelaxed neutral geometry is much more stabilized in COSMO than in TIP3P. Interestingly, despite this dissimilar behaviour between the unrelaxed trajectories for COSMO and TIP3P, the results obtained by the dynamic Marcus protocol in both solvent models are not too different because TIP3P overestimates the VIEs but underestimates the VAEs, making the average of the two magnitudes similar to the one computed with COSMO. However, the slightly better performance of the COSMO calculations is likely explained by the polarizable nature of the solvent model.

Finally, Figure 6 also displays the standard deviations of the QM/TIP3P and QM/-COSMO energy calculations for the relaxed and unrelaxed trajectories. As can be seen, the standard deviations for COSMO are much smaller (0.03–0.04 eV) than those for TIP3P (0.16–0.32 eV). These larger energy oscillations observed for the explicit solvent cause the large standard deviations in the oxidation potentials shown in Figure 5 for both the dynamic direct and dynamic Marcus protocols.

4.3 DFT Functionals

The electronic-structure calculations for the static and dynamic approaches described in this work were carried out using the PBEOP, M06-2X and B3LYP functionals. In general

terms, PBEOP is the functional that presents the best agreement with the experimental oxidation potentials, as can be seen in Figures 3 and 5. In addition, PBEOP provides the lowest one-electron oxidation potentials for the five nucleobases, followed by B3LYP and then by M06-2X, as illustrated in Table 2. For the schemes that describe the solvent with a continuum solvation model, B3LYP and M06-2X give oxidation potentials ~ 0.3 V and ~ 0.5 V, respectively, greater than PBEOP for all nucleobases in both the static and dynamic protocols. These differences between PBEOP and B3LYP become a bit larger when the solvent is explicitly described by TIP3P in the dynamic Marcus protocol, whereas the errors with respect to PBEOP barely change for M06-2X. Specifically, the oxidation potentials computed with M06-2X and B3LYP are $\sim 0.5 - 0.7$ V and $\sim 0.1 - 0.3$ V larger, respectively, than those computed using PBEOP. The only situation where PBEOP does not perform the best is for the dynamic direct explicit protocol, for which M06-2X presents the lowest MUE value (0.39 V), followed by PBEOP (0.86 V) and B3LYP (1.18 V).

If the oxidation potentials of the nucleobases are analyzed individually, PBEOP provides better results for purines (adenine and guanine) than for pyrimidines (cytosine, thymine and uracyl). Actually, PBEOP slightly underestimates the potentials of adenine and guanine in all static and dynamic approaches using implicit solvation (see Table 2 and Figures 3 and 5). In the case of the dynamic direct explicit protocol this underestimation is more important, and the potentials of purines are slightly overestimated in the dynamic Marcus explicit procedure. On the other hand, potentials for cytosine, thymine and uracil are always overestimated by PBEOP, showing larger errors than for purines but still in good agreement with the experimental data. The only exception is found in the dynamic direct explicit approach, where the computed oxidation potentials are much lower than the experimental ones. M06-2X is the functional that presents the largest deviation from the experimental results in both static and dynamic methodologies, with the already mentioned exception of the dynamic direct explicit approach. As in the case of PBEOP, the M06-2X errors found for the purine nucleobases are lower than the errors found for the pyrimidine ones. The

Table 2: Calculated one-electron oxidation potentials using the PBEOP, M06-2X and B3LYP functionals with the 6-311G(d) basis set for each of the static and dynamic approaches: Static direct (SD), static cycle 1 (SC1), static cycle 2 (SC2), dynamic direct implicit (DDI), dynamic direct explicit (DDE), dynamic Marcus implicit (DMI) and dynamic Marcus explicit (DME). All the potentials are given in V.

PBEOP							
N	$E_{red,SD}$	$E_{red,SC1}$	$E_{red,SC2}$	$E_{red,DDI}$	$E_{red,DDE}$	$E_{red,DMI}$	$E_{red,DME}$
A	1.12	1.10	1.11	1.14 ± 0.22	0.17 ± 1.26	1.13 ± 0.07	1.51 ± 0.66
C	1.53	1.69	1.72	1.74 ± 0.50	1.35 ± 1.74	1.74 ± 0.28	2.23 ± 0.83
G	0.85	0.58	0.58	0.86 ± 0.24	0.29 ± 1.78	0.78 ± 0.07	1.27 ± 0.75
T	1.54	2.07	2.04	1.59 ± 0.18	0.40 ± 1.38	1.55 ± 0.07	2.04 ± 0.63
U	1.90	2.62	2.62	1.98 ± 0.22	0.76 ± 1.36	1.88 ± 0.06	2.35 ± 0.70
M06-2X							
N	$E_{red,SD}$	$E_{red,SC1}$	$E_{red,SC2}$	$E_{red,DDI}$	$E_{red,DDE}$	$E_{red,DMI}$	$E_{red,DME}$
A	1.72	1.72	1.73	1.80 ± 0.24	1.02 ± 1.41	1.72 ± 0.09	2.16 ± 0.66
C	2.41	2.15	2.50	2.20 ± 0.32	1.69 ± 1.74	2.33 ± 0.07	2.90 ± 0.73
G	1.41	1.12	1.13	1.41 ± 0.27	0.46 ± 1.75	1.37 ± 0.08	1.77 ± 0.67
T	2.05	2.64	2.64	2.08 ± 0.18	1.11 ± 1.55	2.08 ± 0.09	2.64 ± 0.69
U	2.39	3.28	3.28	2.35 ± 0.19	1.14 ± 1.45	2.41 ± 0.09	2.85 ± 0.73
B3LYP							
N	$E_{red,SD}$	$E_{red,SC1}$	$E_{red,SC2}$	$E_{red,DDI}$	$E_{red,DDE}$	$E_{red,DMI}$	$E_{red,DME}$
A	1.47	1.47	1.48	1.52 ± 0.25	0.45 ± 1.24	1.46 ± 0.07	1.82 ± 0.61
C	2.28	1.64	2.05	2.05 ± 0.28	1.36 ± 1.73	2.02 ± 0.06	2.58 ± 0.73
G	1.17	0.90	0.91	1.19 ± 0.26	2.31 ± 1.78	1.11 ± 0.09	1.25 ± 0.65
T	1.87	2.40	2.40	1.93 ± 0.16	3.50 ± 1.30	1.89 ± 0.09	2.20 ± 0.67
U	2.22	3.05	3.05	2.21 ± 0.20	3.06 ± 1.30	2.21 ± 0.07	2.51 ± 0.71

accuracy of the B3LYP functional is halfway between the one given by PBEOP and M06-2X. Moreover, the error of B3LYP is smaller for purines than for pyrimidines, resembling the behaviour of the other two functionals.

4.4 Tautomerism Effects

The relative order of the one-electron oxidation potentials previously determined by experiments and theory^{1,2,4,5,17,18,26,28,30,31} is successfully reproduced by our calculations using both static and dynamic approaches: $G < A < T < C < U$. Thus, guanine is the most oxidizable nucleobase followed by adenine, i.e., purine molecules are proner than pyrimidines to transfer an electron to a sacrificial agent present in the environment. This can be explained in terms of the degree of electronic delocalization. Since the π system of purine derivatives is larger than the π system of pyrimidine derivatives, the energy needed to detach an electron from the molecule is smaller in purines than in pyrimidines. From a different but equivalent point of view, the positive charge generated when the cation is formed after oxidation can be more easily delocalized over the π system of purines, making the system more stable than a positive charge in pyrimidines.

Although our calculations properly reproduce the relative oxidation potentials of nucleobases, the agreement with the experimental values is not perfect. One possible source of deviation could be related with the fact that only the most stable tautomer has been considered in the different theoretical models. However, several tautomeric species can exist in protic solvents such as water, and they should be taken into account. Hobza and co-workers carried out a systematic theoretical study on the stability of the main tautomers of the nucleobases.⁹⁰⁻⁹³ Here, the relative energies of the different tautomers with respect to the canonical forms have been taken from the works by Hobza *et al.*, and the relative population of each tautomer was calculated assuming a Boltzmann distribution. The one-electron oxidation potentials of the tautomers with a significant population - over 1% - at 298.15 K were calculated using the static direct approach, and the weighted average oxidation potential

was computed for each nucleobase.

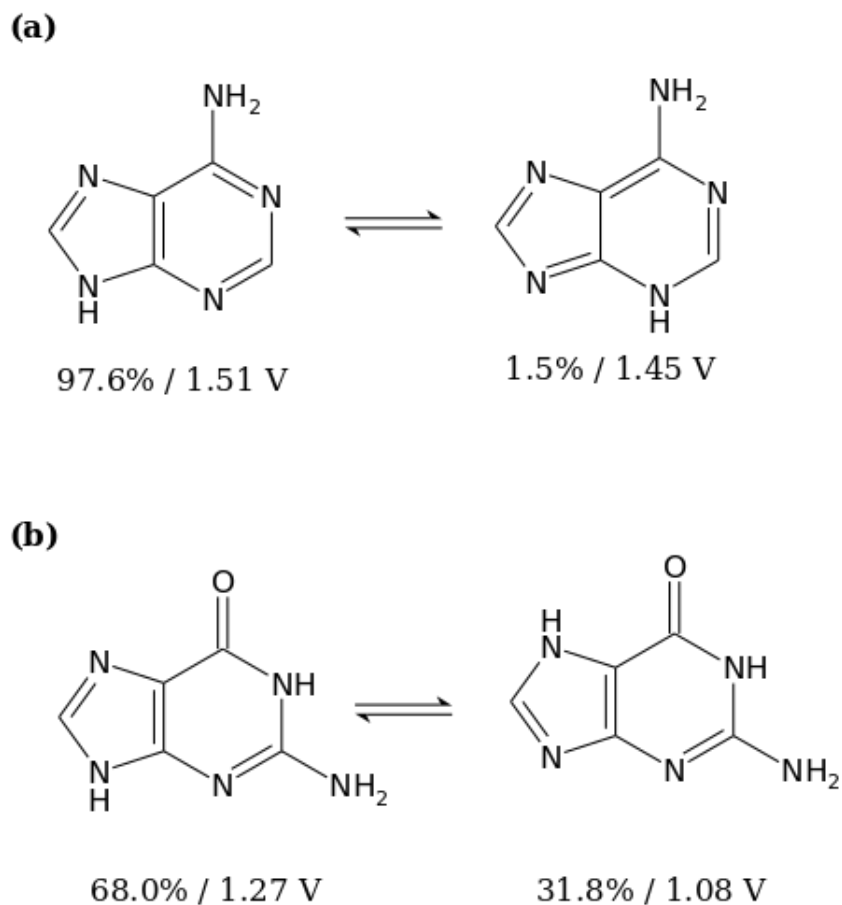


Figure 7: Schematic representation of the relevant tautomers that affect the value of the one-electron oxidation potential of (a) adenine, (b) guanine. Population of each tautomer is calculated using the energies provided by Hobza and co-workers.^{90,92} Computation of the potentials were performed by means of the static direct scheme using PBEOP/6-311G(d)/COSMO.

The relative abundance of all the tautomers of the pyrimidine nucleobases resulted to be insignificant. Therefore, it can be stated that the average one-electron oxidation potentials of these molecules are completely dominated by the potential of the canonical form. In the case of adenine, the abundance of the canonical form is 97.6% ($E_{red} = 1.51$ V), while the non-canonical form with a hydrogen bonded to N3 instead of N9 (see Figure 7) presents an abundance of 1.5% ($E_{red} = 1.45$ V). The weighted average one-electron oxidation potential was 1.50 V, that is, only 0.01 V lower than the potential of the canonical species. This means that tautomerism has no significant effect on adenine. Finally, guanine shows two important

tautomers: the canonical form with a Boltzmann population of 68.0% ($E_{red} = 1.27$ V) and the form where a hydrogen migrated from N9 to N7 with a population of 31.8% ($E_{red} = 1.08$ V). The weighted average one-electron oxidation potential resulted in 1.21 V. Therefore, this evidences that although the guanine potential is slightly altered by the presence of a tautomer, this change is small (0.06 V) and can be ignored. Consequently, the study of one-electron oxidation potentials of the nucleobases can be carried out without taking into account the effect of tautomerism.

5 Conclusions

The establishment of accurate theoretical protocols to compute the redox properties of the nucleobases is of fundamental importance when modeling charge-transfer processes, as those involved in the functioning of DNA-based biosensors. In the present work, different static and dynamic computational models using implicit and explicit solvation have been proposed and evaluated in order to compute the one-electron oxidation potentials of the five nucleobases.

Three static protocols have been employed, including the direct calculation of the oxidation potentials from the AIE (static direct) and two different thermodynamic cycles, where relaxation upon solvation is considered (static cycle 1) or ignored (static cycle 2). The static direct approach provided the most accurate results with respect to the experimental values found in the literature. Both thermodynamic cycles gave similar results for all nucleobases but cytosine, for which the static cycle 1 performed better, indicating that geometry relaxation upon solvation is relatively relevant only for this particular nucleobase.

Vibrational sampling was introduced in the model by running classical MD simulations for the neutral and cationic solvated species. Then, the oxidation potential was computed directly from the energy difference between the two trajectories (dynamic direct protocol) or from the average of the VIE and VAE (dynamic Marcus protocol). The energy calculations were performed for 200 snapshots, selected from each of the trajectories, in the implicit

COSMO and explicit TIP3P solvent models by polarizable-embedding QM/continuum and electrostatic-embedding QM/MM schemes. All the dynamic protocols have shown to be converged after using 100 snapshots. The application of the Marcus theory provided faster convergence than the use of the direct approach. In addition, the use of COSMO also showed a better convergence behaviour than the calculations carried out with TIP3P.

The comparison of the oxidation potentials obtained by the static protocols and by the dynamic ones in implicit solvation revealed that sampling effects are not important since static and dynamic implicit calculations gave very similar results. This is particularly relevant considering that the calculation of the oxidation potential for a nucleobase by the static direct approach requires to run solely two geometry optimizations and two frequency calculations, while the application of a dynamic protocol requires to run two classical MD simulations followed by 400 (800) single-point calculations for the direct (Marcus) approach. Therefore, the static approximations are computationally much cheaper and simpler than the dynamic ones.

The effect of using different solvation models was investigated in the dynamic framework. In general, the errors obtained in explicit solvent were larger than those obtained in implicit solvent. This demonstrated that the introduction of mutual polarization between the solute and solvent is important to obtain more accurate results. In addition, due to the nature of the COSMO model, where all possible solvent configurations are represented by the cavity in an average way in each single-point calculation, the standard deviations of the oxidation potentials along the geometries of the ensembles are much smaller in COSMO than in TIP3P. Moreover, the use of the Marcus theory improved the results obtained by the dynamic direct approach when using explicit solvent, but not the implicit one, for which the accuracy of both dynamic protocols are very similar.

Three different functionals, namely PBEOP, M06-2X and B3LYP, have been employed for all static and dynamic protocols. In general, PBEOP is the functional that provided the lowest oxidation potentials and the best agreement with the experimental values for all

the protocols but the dynamic direct explicit approach. In this particular case, fortuitous error cancellation makes M06-2X the best choice to describe the electronic structure of the nucleobases. Finally, the presence of different tautomers in water is only relatively relevant for adenine and guanine, but their inclusion in the theoretical model did not significantly influence the values of the one-electron oxidation potentials.

In summary, the most accurate computational protocols to compute the one-electron oxidation potentials of nucleobases in water are the static direct, dynamic direct implicit and dynamic Marcus implicit calculations. Although the static approach seems, thus, the obvious choice due to its computational efficiency and simplicity, it is important to keep in mind that the use of dynamic approaches will likely be necessary when modeling more complex systems, such a biosensor formed by several DNA strands linked to a metal surface. In addition, the inclusion of explicit solvent molecules in the model could also be necessary if specific interactions, e.g., hydrogen bonding, play an important role in such devices.

Acknowledgement

We acknowledge the generous allocation of computer time at the Centro de Computación Científica at the Universidad Autónoma de Madrid (CCC-UAM). This work was partially supported by the MICINN - Spanish Ministry of Science and Innovation – Projects PID2019-110091GB-I00 and PID2020-117806GA-I00 funded by MCIN/AEI/10.13039/501100011033, and the 'María de Maeztu' (CEX2018-000805-M) Program for Centers of Excellence in R&D. J.J.N. and G.C. acknowledge the Comunidad de Madrid for funding through the Attraction of Talent Program (Grant ref 2018-T1/BMD-10261). N.A.O. acknowledges the Comunidad de Madrid and European Social Fund for funding through the Programa Operativo de Empleo Juvenil y la Iniciativa de Empleo Juvenil. J.L.T. acknowledges the FPU-2019 grant from the Spanish Ministry of Education.

References

- (1) D'Annibale, V.; Nardi, A. N.; Amadei, A.; D'Abramo, M. Theoretical Characterization of the Reduction Potentials of Nucleic Acids in Solution. *Journal of Chemical Theory and Computation* **2021**, *17*, 1301–1307.
- (2) Psciuk, B. T.; Lord, R. L.; Munk, B. H.; Schlegel, H. B. Theoretical Determination of One-Electron Oxidation Potentials for Nucleic Acid Bases. *Journal of Chemical Theory and Computation* **2012**, *8*, 5107–5123.
- (3) Faraggi, M.; Broitman, F.; Trent, J. B.; Klapper, M. H. One-Electron Oxidation Reactions of Some Purine and Pyrimidine Bases in Aqueous Solutions. Electrochemical and Pulse Radiolysis Studies. *The Journal of Physical Chemistry* **1996**, *100*, 14751–14761.
- (4) Jovanovic, S. V.; Simic, M. G. One-electron redox potentials of purines and pyrimidines. *The Journal of Physical Chemistry* **1986**, *90*, 974–978.
- (5) Seidel, C. A. M.; Schulz, A.; Sauer, M. H. M. Nucleobase-Specific Quenching of Fluorescent Dyes. 1. Nucleobase One-Electron Redox Potentials and Their Correlation with Static and Dynamic Quenching Efficiencies. *The Journal of Physical Chemistry* **1996**, *100*, 5541–5553.
- (6) Ghoshdastidar, D.; Ghosh, D.; Senapati, S. High Nucleobase-Solubilizing Ability of Low-Viscous Ionic Liquid/Water Mixtures: Measurements and Mechanism. *The Journal of Physical Chemistry B* **2016**, *120*, 492–503.
- (7) Mehrotra, P. Biosensors and their applications – A review. *Journal of Oral Biology and Craniofacial Research* **2016**, *6*, 153–159.
- (8) Kissinger, P. T. Biosensors—a perspective. *Biosensors and Bioelectronics* **2005**, *20*, 2512–2516.

- (9) Zhai, J.; Cui, H.; Yang, R. DNA based biosensors. *Biotechnology Advances* **1997**, *15*, 43–58.
- (10) Ozkan, D.; Erdem, A.; Kara, P.; Kerman, K.; Meric, B.; Hassmann, J.; Ozsoz, M. Allele-Specific Genotype Detection of Factor V Leiden Mutation from Polymerase Chain Reaction Amplicons Based on Label-Free Electrochemical Genosensor. *Analytical Chemistry* **2002**, *74*, 5931–5936.
- (11) Wong, E. L.; Mearns, F. J.; Gooding, J. J. Further development of an electrochemical DNA hybridization biosensor based on long-range electron transfer. *Sensors and Actuators: B. Chemical* **2005**, *111-112*, 515–521.
- (12) Sadik, O. A.; Aluoch, A. O.; Zhou, A. Status of biomolecular recognition using electrochemical techniques. *Biosensors and Bioelectronics* **2009**, *24*, 2749–2765.
- (13) Saidur, M.; Aziz, A. A.; Basirun, W. Recent advances in DNA-based electrochemical biosensors for heavy metal ion detection: A review. *Biosensors and Bioelectronics* **2017**, *90*, 125–139.
- (14) Bu, N.-N.; Tang, C.-X.; He, X.-W.; Yin, X.-B. Tetrahedron-structured DNA and functional oligonucleotide for construction of an electrochemical DNA-based biosensor. *Chemical Communications* **2011**, *47*, 7689–7691.
- (15) Berlin, Y. A.; Burin, A. L.; Ratner, M. A. DNA as a molecular wire. *Superlattices and Microstructures* **2000**, *28*, 241–252.
- (16) Wohlgamuth, C. H.; McWilliams, M. A.; Slinker, J. D. DNA as a Molecular Wire: Distance and Sequence Dependence. *Analytical Chemistry* **2013**, *85*, 8634–8640.
- (17) Steenken, S.; Jovanovic, S. V. How Easily Oxidizable Is DNA? One-Electron Reduction Potentials of Adenosine and Guanosine Radicals in Aqueous Solution. *Journal of the American Chemical Society* **1997**, *119*, 617–618.

- (18) Steenken, S.; Jovanovic, S. V.; Bietti, M.; Bernhard, K. The Trap Depth (in DNA) of 8-Oxo-7,8-dihydro-2'-deoxyguanosine as Derived from Electron-Transfer Equilibria in Aqueous Solution. *Journal of the American Chemical Society* **2000**, *122*, 2373–2374.
- (19) Burrows, C. J.; Muller, J. G. Oxidative Nucleobase Modifications Leading to Strand Scission. *Chemical Reviews* **1998**, *98*, 1109–1152.
- (20) Steenken, S. Purine bases, nucleosides, and nucleotides: aqueous solution redox chemistry and transformation reactions of their radical cations and e- and OH adducts. *Chemical Reviews* **1989**, *89*, 503–520.
- (21) Kittler, L.; Löber, G.; Gollmick, F.; Berg, H. Redox processes during photodynamic damage of DNA. *Journal of Electroanalytical Chemistry and Interfacial Electrochemistry* **1980**, *116*, 503–511.
- (22) Reipa, V.; Atha, D. H.; Coskun, S. H.; Sims, C. M.; Nelson, B. C. Controlled potential electro-oxidation of genomic DNA. *PLOS ONE* **2018**, *13*, 1–18.
- (23) Xie, H.; Yang, D.; Heller, A.; Gao, Z. Electrocatalytic Oxidation of Guanine, Guanosine, and Guanosine Monophosphate. *Biophysical Journal* **2007**, *92*, L70–L72.
- (24) Min-Jie, L.; Wei-Xia, L.; Chun-Rong, P.; Wen-Cong, L. A First-Principles Method for Predicting Redox Potentials of Nucleobases and the Metabolites in Aqueous Solution. *Acta Physico-Chimica Sinica* **2011**, *27*, 595–603.
- (25) Baik, M.-H.; Silverman, J. S.; Yang, I. V.; Ropp, P. A.; Szalai, V. A.; Yang, W.; Thorp, H. H. Using Density Functional Theory To Design DNA Base Analogues with Low Oxidation Potentials. *The Journal of Physical Chemistry B* **2001**, *105*, 6437–6444.
- (26) Zhang, Y.; Xie, P.; Yang, S.; Han, K. Ionization and Electron Attachment for Nucleobases in Water. *The Journal of Physical Chemistry B* **2019**, *123*, 1237–1247.

- (27) Thapa, B.; Schlegel, H. B. Calculations of pKa's and Redox Potentials of Nucleobases with Explicit Waters and Polarizable Continuum Solvation. *The Journal of Physical Chemistry A* **2015**, *119*, 5134–5144.
- (28) Paukku, Y.; Hill, G. Theoretical Determination of One-Electron Redox Potentials for DNA Bases, Base Pairs, and Stacks. *The Journal of Physical Chemistry A* **2011**, *115*, 4804–4810.
- (29) Lewis, K.; Copeland, K.; Hill, G. One-Electron Redox Properties of DNA Nucleobases and Common Tautomers. *International Journal of Quantum Chemistry* **2014**, *114*, 1678–1684.
- (30) Wang, J.; Yang, S.; Zhang, Y. One-electron oxidation and redox potential of nucleobases and deoxyribonucleosides computed by QM/MM simulations. *Chemical Physics Letters* **2020**, *739*, 136948.
- (31) Crespo-Hernández, C. E.; Close, D. M.; Gorb, L.; Leszczynski, J. Determination of Redox Potentials for the Watson-Crick Base Pairs, DNA Nucleosides, and Relevant Nucleoside Analogues. *The Journal of Physical Chemistry B* **2007**, *111*, 5386–5395.
- (32) Adcock, S. A.; McCammon, J. A. Molecular Dynamics: Survey of Methods for Simulating the Activity of Proteins. *Chemical Reviews* **2006**, *106*, 1589–1615.
- (33) Braun, E.; Gilmer, J.; Mayes, H. B.; Mobley, D. L.; Monroe, J. I.; Prasad, S.; Zuckerman, D. M. Best Practices for Foundations in Molecular Simulations [Article v1.0]. *Living Journal of Computational Molecular Science* **2018**, *1*, 5957–5957.
- (34) Senn, H. M.; Thiel, W. QM/MM Methods for Biomolecular Systems. *Angewandte Chemie International Edition* **2009**, *48*, 1198–1229.
- (35) Jorgensen, W. L.; Chandrasekhar, J.; Madura, J. D.; Impey, R. W.; Klein, M. L.

- Comparison of simple potential functions for simulating liquid water. *The Journal of Chemical Physics* **1983**, *79*, 926–935.
- (36) Aschi, M.; Spezia, R.; Nola, A.; Amadei, A. A first-principles method to model perturbed electronic wavefunctions: The effect of an external homogeneous electric field. *Chemical Physics Letters* **2001**, *344*, 374–380.
- (37) Zanetti-Polzi, L.; Del Galdo, S.; Daidone, I.; D’Abramo, M.; Barone, V.; Aschi, M.; Amadei, A. Extending the perturbed matrix method beyond the dipolar approximation: comparison of different levels of theory. *Physical Chemistry Chemical Physics* **2018**, *20*, 24369–24378.
- (38) Ho, J. Are thermodynamic cycles necessary for continuum solvent calculation of pK_as and reduction potentials? *Physical Chemistry Chemical Physics* **2015**, *17*, 2859–2868.
- (39) Miertus, S.; Scrocco, E.; Tomasi, J. Electrostatic interaction of a solute with a continuum. A direct utilization of AB initio molecular potentials for the prediction of solvent effects. *Chemical Physics* **1981**, *55*, 117–129.
- (40) Miertus, S.; Tomasi, J. Approximate evaluations of the electrostatic free energy and internal energy changes in solution processes. *Chemical Physics* **1982**, *65*, 239–245.
- (41) Pascual-Ahuir, J. L.; Silla, E.; Tuñón, I. GEPOL: An improved description of molecular surfaces. III. A new algorithm for the computation of a solvent-excluding surface. *Journal of Computational Chemistry* **1994**, *15*, 1127–1138.
- (42) Barone, V.; Cossi, M.; Tomasi, J. A new definition of cavities for the computation of solvation free energies by the polarizable continuum model. *The Journal of Chemical Physics* **1997**, *107*, 3210–3221.
- (43) Cancès, E.; Mennucci, B.; Tomasi, J. A new integral equation formalism for the po-

- larizable continuum model: Theoretical background and applications to isotropic and anisotropic dielectrics. *The Journal of Chemical Physics* **1997**, *107*, 3032–3041.
- (44) Mennucci, B.; Tomasi, J.; Cammi, R.; Cheeseman, J. R.; Frisch, M. J.; Devlin, F. J.; Gabriel, S.; Stephens, P. J. Polarizable Continuum Model (PCM) Calculations of Solvent Effects on Optical Rotations of Chiral Molecules. *The Journal of Physical Chemistry A* **2002**, *106*, 6102–6113.
- (45) Klamt, A.; Schüürmann, G. COSMO: a new approach to dielectric screening in solvents with explicit expressions for the screening energy and its gradient. *About Journal of the Chemical Society, Perkin Transactions 2* **1993**, 799–805.
- (46) York, D. M.; Karplus, M. A Smooth Solvation Potential Based on the Conductor-Like Screening Model. *The Journal of Physical Chemistry A* **1999**, *103*, 11060–11079.
- (47) Bartmess, J. E. Thermodynamics of the Electron and the Proton. *The Journal of Physical Chemistry* **1994**, *98*, 6420–6424.
- (48) Bartmess, J. E. Erratum: Thermodynamics of the Electron and the Proton (Journal of Physical Chemistry (1994) 98 (6420-6424)). *The Journal of Physical Chemistry* **1995**, *99*, 6755–6755.
- (49) Truhlar, D. G.; Cramer, C. J.; Lewis, A.; Bumpus, J. A. Molecular Modeling of Environmentally Important Processes: Reduction Potentials. *Journal of Chemical Education* **2004**, *81*, 596–604.
- (50) Truhlar, D. G.; Cramer, C. J.; Lewis, A.; Bumpus, J. A. Erratum: Molecular modeling of environmentally important processes: Reduction potentials (Journal of Chemical Education (2004) 81 (596-604)). *Journal of Chemical Education* **2007**, *84*, 934–934.
- (51) Isse, A. A.; Gennaro, A. Absolute Potential of the Standard Hydrogen Electrode and the

- Problem of Interconversion of Potentials in Different Solvents. *The Journal of Physical Chemistry B* **2010**, *114*, 7894–7899.
- (52) Kelly, C. P.; Cramer, C. J.; Truhlar, D. G. Aqueous Solvation Free Energies of Ions and Ion-Water Clusters Based on an Accurate Value for the Absolute Aqueous Solvation Free Energy of the Proton. *The Journal of Physical Chemistry B* **2006**, *110*, 16066–16081.
- (53) Warshel, A. Dynamics of reactions in polar solvents. Semiclassical trajectory studies of electron-transfer and proton-transfer reactions. *The Journal of Physical Chemistry* **1982**, *86*, 2218–2224.
- (54) King, G.; Warshel, A. Investigation of the free energy functions for electron transfer reactions. *The Journal of Chemical Physics* **1990**, *93*, 8682–8692.
- (55) Blumberger, J.; Tavernelli, I.; Klein, M. L.; Sprik, M. Diabatic free energy curves and coordination fluctuations for the aqueous Ag⁺/Ag²⁺ redox couple: A biased Born-Oppenheimer molecular dynamics investigation. *The Journal of Chemical Physics* **2006**, *124*, 064507.
- (56) Zwanzig, R. W. High-Temperature Equation of State by a Perturbation Method. I. Nonpolar Gases. *The Journal of Chemical Physics* **1954**, *22*, 1420–1426.
- (57) Marcus, R. A. On the Theory of Oxidation-Reduction Reactions Involving Electron Transfer. I. *The Journal of Chemical Physics* **1956**, *24*, 966–978.
- (58) Marcus, R. A. On the Theory of Oxidation-Reduction Reactions Involving Electron Transfer. III. Applications to Data on the Rates of Organic Redox Reactions. *Journal of Chemical Physics* **1957**, *26*, 872–877.
- (59) Marcus, R. A. On the Theory of Oxidation-Reduction Reactions Involving Electron

- Transfer. V. Comparison and Properties of Electrochemical and Chemical Rate Constants. *The Journal of Physical Chemistry* **1963**, *67*, 853–857.
- (60) Marcus, R. A. On the theory of electron-transfer reactions. VI. Unified treatment for homogeneous and electrode reactions. *The Journal of Chemical Physics* **1965**, *43*, 679–701.
- (61) Cárdenas, G.; Marquetand, P.; Mai, S.; González, L. A Force Field for a Manganese–Vanadium Water Oxidation Catalyst: Redox Potentials in Solution as Showcase. *Catalysts* **2021**, *11*, 493.
- (62) Valiev, M.; Bylaska, E. J.; Govind, N.; Kowalski, K.; Straatsma, T. P.; Van Dam, H. J. J.; Wang, D.; Nieplocha, J.; Apra, E.; Windus, T. L.; de Jong, W. A. NWChem: A comprehensive and scalable open-source solution for large scale molecular simulations. *Computer Physics Communications* **2010**, *181*, 1477–1489.
- (63) Perdew, J. P.; Burke, K.; Ernzerhof, M. Generalized Gradient Approximation Made Simple. *Physical Review Letters* **1996**, *77*, 3865–3868.
- (64) Perdew, J. P.; Burke, K.; Ernzerhof, M. Erratum: Generalized gradient approximation made simple (Physical Review Letters (1996) 77 (3865)). *Physical Review Letters* **1997**, *78*, 1396–1396.
- (65) Tsuneda, T.; Suzumura, T.; Hirao, K. A new one-parameter progressive Colle–Salvetti-type correlation functional. *The Journal of Chemical Physics* **1999**, *110*, 10664–10678.
- (66) Sarmah, P.; Deka, R. C. Density functional studies on the electron affinities of DNA and RNA bases. *Molecular Simulation* **2008**, *34*, 879–885.
- (67) Becke, A. D. Density-functional thermochemistry. III. The role of exact exchange. *The Journal of Chemical Physics* **1993**, *98*, 5648–5652.

- (68) Lee, C.; Yang, W.; Parr, R. G. Development of the Colle-Salvetti correlation-energy formula into a functional of the electron density. *Physical Review B* **1988**, *37*, 785–789.
- (69) Stephens, P. J.; Devlin, F. J.; Chabalowski, C. F.; Frisch, M. J. Ab Initio Calculation of Vibrational Absorption and Circular Dichroism Spectra Using Density Functional Force Fields. *The Journal of Physical Chemistry* **1994**, *98*, 11623–11627.
- (70) Vosko, S. H.; Wilk, L.; Nusair, M. Accurate spin-dependent electron liquid correlation energies for local spin density calculations: a critical analysis. *Canadian Journal of Physics* **1980**, *58*, 1200–1211.
- (71) Zhao, Y.; Truhlar, D. The M06 suite of density functionals for main group thermochemistry, thermochemical kinetics, noncovalent interactions, excited states, and transition elements: Two new functionals and systematic testing of four M06-class functionals and 12 other functionals. *Theoretical Chemistry Accounts* **2008**, *120*, 215–241.
- (72) Petersson, G. A.; Bennett, A.; Tensfeldt, T. G.; Al-Laham, M. A.; Shirley, W. A.; Mantzaris, J. A complete basis set model chemistry. I. The total energies of closed-shell atoms and hydrides of the first-row elements. *The Journal of Chemical Physics* **1988**, *89*, 2193–2218.
- (73) Petersson, G. A.; Al-Laham, M. A. A complete basis set model chemistry. II. Open-shell systems and the total energies of the first-row atoms. *The Journal of Chemical Physics* **1991**, *94*, 6081–6090.
- (74) D.A. Case, H.M. Aktulga, K. Belfon, I.Y. Ben-Shalom, S.R. Brozell, D.S. Cerutti, T.E. Cheatham, III, G.A. Cisneros, V.W.D. Cruzeiro, T.A. Darden, R.E. Duke, G. Giambasu, M.K. Gilson, H. Gohlke, A.W. Goetz, R. Harris, S. Izadi, S.A. Izmailov, C. Jin, K. Kasavajhala, M.C. Kaymak, E. King, A. Kovalenko, T. Kurtzman, T.S. Lee, S. LeGrand, P. Li, C. Lin, J. Liu, T. Luchko, R. Luo, M. Machado, V. Man, M. Manathunga, K.M. Merz, Y. Miao, O. Mikhailovskii, G. Monard, H. Nguyen, K.A. O’Hearn,

- A. Onufriev, F. Pan, S. Pantano, R. Qi, A. Rahnamoun, D.R. Roe, A. Roitberg, C. Sagui, S. Schott-Verdugo, J. Shen, C.L. Simmerling, N.R. Skrynnikov, J. Smith, J. Swails, R.C. Walker, J. Wang, H. Wei, R.M. Wolf, X. Wu, Y. Xue, D.M. York, S. Zhao, and P.A. Kollman (2021), Amber 2021, University of California, San Francisco.
- (75) Seminario, J. M. Calculation of intramolecular force fields from second-derivative tensors. *International Journal of Quantum Chemistry* **1996**, *60*, 1271–1277.
- (76) Wang, J.; Wolf, R. M.; Caldwell, J. W.; Kollman, P. A.; Case, D. A. Development and testing of a general amber force field. *Journal of Computational Chemistry* **2004**, *25*, 1157–1174.
- (77) Joung, I. S.; Cheatham, T. E. Determination of Alkali and Halide Monovalent Ion Parameters for Use in Explicitly Solvated Biomolecular Simulations. *The Journal of Physical Chemistry B* **2008**, *112*, 9020–9041.
- (78) Meza, J. C. Steepest descent. *WIREs Computational Statistics* **2010**, *2*, 719–722.
- (79) Galántai, A. The theory of Newton’s method. *Journal of Computational and Applied Mathematics* **2000**, *124*, 25–44.
- (80) Darden, T.; York, D.; Pedersen, L. Particle Mesh Ewald: An N·log(N) Method for Ewald Sums in Large Systems. *Journal of Chemical Physics* **1993**, *98*, 10089–10092.
- (81) Ryckaert, J.-P.; Ciccotti, G.; Berendsen, H. J. Numerical integration of the cartesian equations of motion of a system with constraints: molecular dynamics of n-alkanes. *Journal of Computational Physics* **1977**, *23*, 327–341.
- (82) Hammonds, K. D.; Heyes, D. M. Shadow Hamiltonian in classical NVE molecular dynamics simulations: A path to long time stability. *The Journal of Chemical Physics* **2020**, *152*, 024114.

- (83) Yoneya, M.; Berendsen, H. J. C.; Hirasawa, K. A Non-Iterative Matrix Method for Constraint Molecular Dynamics Simulations. *Molecular Simulation* **1994**, *13*, 395–405.
- (84) Nogueira, J. J.; Plasser, F.; González, L. Electronic delocalization, charge transfer and hypochromism in the UV absorption spectrum of polyadenine unravelled by multiscale computations and quantitative wavefunction analysis. *Chemical Science* **2017**, *8*, 5682–5691.
- (85) Nogueira, J. J.; González, L. Computational Photophysics in the Presence of an Environment. *Annual Review of Physical Chemistry* **2018**, *69*, 473–497.
- (86) Zobel, J. P.; Heindl, M.; Nogueira, J. J.; González, L. Vibrational Sampling and Solvent Effects on the Electronic Structure of the Absorption Spectrum of 2-Nitronaphthalene. *Journal of Chemical Theory and Computation* **2018**, *14*, 3205–3217.
- (87) Zobel, J. P.; Nogueira, J. J.; González, L. Finite-temperature Wigner phase-space sampling and temperature effects on the excited-state dynamics of 2-nitronaphthalene. *Physical Chemistry Chemical Physics* **2019**, *21*, 13906–13915.
- (88) Nogueira, J. J.; Roßbach, S.; Ochsenfeld, C.; González, L. Effect of DNA Environment on Electronically Excited States of Methylene Blue Evaluated by a Three-Layered QM/QM/MM ONIOM Scheme. *Journal of Chemical Theory and Computation* **2018**, *14*, 4298–4308.
- (89) De Vetta, M.; Menger, M. F. S. J.; Nogueira, J. J.; González, L. Solvent Effects on Electronically Excited States: QM/Continuum Versus QM/Explicit Models. *The Journal of Physical Chemistry B* **2018**, *122*, 2975–2984.
- (90) Hanus, M.; Kabeláč, M.; Rejnek, J.; Ryjáček, F.; Hobza, P. Correlated ab Initio Study of Nucleic Acid Bases and Their Tautomers in the Gas Phase, in a Microhydrated Environment, and in Aqueous Solution. Part 3. Adenine. *The Journal of Physical Chemistry B* **2004**, *108*, 2087–2097.

- (91) Trygubenko, S. A.; Bogdan, T. V.; Rueda, M.; Orozco, M.; Luque, F. J.; Šponer, J.; Slavíček, P.; Hobza, P. Correlated ab initio study of nucleic acid bases and their tautomers in the gas phase, in a microhydrated environment and in aqueous solution Part 1. Cytosine. *Physical Chemistry Chemical Physics* **2002**, *4*, 4192–4203.
- (92) Hanus, M.; Ryjáček, F.; Kabeláč, M.; Kubař, T.; Bogdan, T. V.; Trygubenko, S. A.; Hobza, P. Correlated ab Initio Study of Nucleic Acid Bases and Their Tautomers in the Gas Phase, in a Microhydrated Environment and in Aqueous Solution. Guanine: Surprising Stabilization of Rare Tautomers in Aqueous Solution. *Journal of the American Chemical Society* **2003**, *125*, 7678–7688.
- (93) Rejnek, J.; Hanus, M.; Kabeláč, M.; Ryjáček, F.; Hobza, P. Correlated ab initio study of nucleic acid bases and their tautomers in the gas phase, in a microhydrated environment and in aqueous solution. Part 4. Uracil and thymine. *Physical Chemistry Chemical Physics* **2005**, *7*, 2006–2017.